

Deep-6DPose: Recovering 6D Object Pose from a Single RGB Image

Thanh-Toan Do, Ming Cai, Trung Pham, Ian Reid
The University of Adelaide, Australia

Abstract—Detecting objects and their 6D poses from only RGB images is an important task for many robotic applications. While deep learning methods have made significant progress in visual object detection and segmentation, the object pose estimation task is still challenging. In this paper, we introduce an end-to-end deep learning framework, named *Deep-6DPose*, that jointly detects, segments, and most importantly recovers 6D poses of object instances from a single RGB image. In particular, we extend the recent state-of-the-art instance segmentation network *Mask R-CNN* with a novel pose estimation branch to directly regress 6D object poses without any post-refinements. Our key technical contribution is the **decoupling of pose parameters into translation and rotation** so that the rotation can be regressed via a Lie algebra representation. The resulting **pose regression loss is differential and unconstrained, making the training tractable**. The experiments on two standard pose benchmarking datasets show that our proposed approach compares favorably with the state-of-the-art RGB-based multi-stage pose estimation methods. Importantly, due to the end-to-end architecture, *Deep-6DPose* is considerably faster than competing multi-stage methods, offers an inference speed of **10 fps** that is well suited for robotic applications.

I. INTRODUCTION

Detecting objects and their 6D poses (3D location and orientation) is an important task for many robotic applications including object manipulations (e.g., pick and place), parts assembly, to name a few. In clutter environments, objects must be first detected before their poses can be estimated. Accurate object segmentation is also important, especially when objects are occluded. Our goal is to develop a deep learning framework that **jointly detects, segments, and most importantly recovers 6D poses of object instances from a single RGB image**. While the first two tasks are getting more and more mature thanks to the power of deep learning, **the 6D pose estimation problem remains a challenging problem**.

Traditional object pose estimation methods are mainly based on the matching of hand-crafted local features (e.g. SIFT [22]). However, these local feature matching based approaches are only suitable for richly textured objects. For poorly textured objects, template-based matching [10, 31, 28] or dense feature learning approaches are usually used [4, 17, 24, 18]. However, the template-based methods are usually sensitive to illuminations and occlusions. The feature learning approaches [4, 17, 24, 18] have shown better performances against template-based methods, but they suffer from several disadvantages, i.e., they require a time-consuming multi-stage processing for learning dense features, generating coarse pose hypotheses, and refining the coarse poses.

With the rising of deep learning, especially Convolutional Neural Networks (CNN), the object classification [16], object detection [7, 27], and recently object instance segmentation [9, 6] tasks have achieved remarkable improvements. However, the application of CNN to 6D object pose estimation problem is still limited. Recently, there are few works [13, 25, 33] which **apply deep learning for 6D object pose estimation**. These methods, however, are not end-to-end or only estimate a coarse object poses. They require further post-refinements to improve the accuracy, which linearly increases the running time, w.r.t. the number of detected objects.

Recently, Mask R-CNN [9] achieves state-of-the-art results in the instance segmentation problem. The key component of Mask R-CNN is a Region Proposal Network (RPN) [27], which predicts multiple object (bounding boxes) proposals in an image at different shapes and sizes. Mask R-CNN further segments instances inside bounding boxes produced from RPN by using additional convolutional layers.

Inspired by the impressive results of Mask R-CNN for object instance segmentation, we are motivated to find the answer for the question that, *can we exploit the merits of RPN to not only segment but also recover the poses of object instances in a single RGB image, in an end-to-end fashion?* To this end, we design a network which simultaneously detects¹, segments, and also recovers 6D poses of object instances from a single RGB image. In particular, we propose a Deep-6DPose network, which goes beyond Mask R-CNN by adding a novel branch for regressing the poses for the object instances inside bounding boxes produced by RPN. The proposed pose branch is parallel with the detection and segmentation branches.

Our main contribution is a novel object pose regressor, where the network regresses translation and rotation parameters separately. Cares must be taken when regressing 3D rotation matrices as not all 3×3 matrices are valid rotation matrices. To work around, we resort to the **Lie algebra** associated with the $SO(3)$ Lie group for our 3D rotation representation. Compared to other representations such as quaternion or orthonormal matrix, Lie algebra is an optimal choice as it is less parameters and unconstrained, thus making the training process easier. Although the Lie algebra representation has been widely used in geometry-based robot vision problems [1, 29], to our best knowledge, this is the first work which successfully uses the Lie algebra in a CNN for

¹The detection means the prediction of both bounding boxes and class labels.

当回归3D旋转矩阵时必须小心，因为并非所有 3×3 矩阵都是有效的旋转矩阵。

regressing 6D object poses.

Different from recent deep learning-based 6D pose estimation methods which are not end-to-end trainable [25] or only predict a rough pose followed by a pose refinement step [13, 25, 33], the proposed Deep-6DPose is a single deep learning architecture. It takes a RGB image as input and directly outputs 6D object poses without any pose post-refinements. Additionally, our system also returns segmentation masks of object instances. The experimental results show that Deep-6DPose is competitive or outperforms the state-of-the-art methods on standard datasets. Furthermore, Deep-6DPose is simple and elegant, allows the inference at the speed of 10 fps, which is several times faster than many existing methods.

The remainder of this paper is organized as follows. Section II presents related works. Section III details the proposed Deep-6DPose. Section IV evaluates and compares Deep-6DPose to the state-of-the-art 6D object pose estimation methods. Section V concludes the paper.

II. RELATED WORK

In this section, we first review the 6D object pose estimation methods. We then brief the main design of the recent methods which are based on RPN for object detection and segmentation.

Classical approaches. The topic of pose estimation has great attention in the past few years. For objects with rich of texture, sparse feature matching approaches have been shown good accuracy [8, 22, 23]. Recently, researchers have put more focus on poor texture or texture-less objects. The most traditional approaches for poor texture objects are to use object templates [10, 31, 28]. The most notable work belonging to this category is LINEMOD [10] which is based on stable gradient and normal features. However, LINEMOD is designed to work with RGBD images. Furthermore, template-based approaches are sensitive to the lighting and occlusion.

Feature learning approach. Recent 6D pose estimation researches have relied on feature learning for dealing with insufficient texture objects [4, 17, 24, 18]. In [4, 17], the authors show that the dense feature learning approach outperforms matching approach. The basic design of [4, 17, 24, 18] is a time-consuming multi-stage pipeline, i.e., a random forest is used for jointly learning the object categories for pixels and the coordinates of pixels w.r.t. object coordinate systems (known as object coordinates). A set of pose hypotheses is generated by using the outputs of the forest and the depth channel of the input image. An energy function is defined on the generated pose hypotheses to select hypotheses. The selected pose hypotheses are further refined to obtain the final pose. Note that the pipelines in those works heavily depend on the depth channel. The depth information is required in both pose hypothesis generation and refinement. The work [5] also follows a multi-stage approach as [4, 17] but is designed to work with RGB inputs. In order to deal with the missing depth information, the distribution of object coordinates is approximated as a mixture model when generating pose hypotheses.

CNN-based approach. In recent years, CNN has been applied for 6D pose problem, firstly for camera pose [15, 14], and recently for object pose [17, 18, 13, 25, 33, 32].

In [15, 14], the authors train CNNs to directly regress 6D camera pose from a single RGB image. The camera pose estimation task is arguably easier than the object pose estimation task, because to estimate object pose, it also requires accurate detection and classification of the object, while these steps are not typically needed for camera pose.

In [17], the authors use a CNN in their object pose estimation system. However, the CNN is only used as a probabilistic model to learn to compare the learned information (produced by a random forest) and the rendered image. The CNN outputs an energy value for selecting pose hypotheses which are further refined. The work in [18] improves over [17] by using a CNN and reinforcement learning for joint selecting and refining pose hypotheses.

In SSD-6D [13], the authors extend SSD detection framework [20] to 3D detection and 3D rotation estimation. The authors decompose 3D rotation space into discrete viewpoints and in-plane rotations. They then treat the rotation estimation as a classification problem. However, to get the good results, it is required to manually find an appropriate sampling for the rotation space. Furthermore, the approach SSD-6D does not directly output the translation, i.e., to estimate the translation, for each object, an offline stage is required to precomputes bounding boxes w.r.t. all possible sampled rotations. This precomputed information is used together with the estimated bounding box and rotation to estimate the 3D translation. In the recent technical report [33], the authors propose a network, dubbed PoseCNN, which jointly segments objects and estimates the rotation and the distance of segmented objects to camera. However, by relying on a semantic segmentation approach (which is a FCN [21]) to localize objects, it may be difficult for PoseCNN to deal with input image which contains multiple instances of an object. Both SSD-6D and PoseCNN also require further pose refinement steps to improve the accuracy.

In BB8 [25], the authors propose a cascade of multiple CNNs for object pose estimation task. A segmentation network is firstly applied to the input image to localize objects. Another CNN is then used to predict 2D projections of the corners of the 3D bounding boxes around objects. The 6D pose is estimated for the correspondences between the projected 2D coordinates and the 3D ground control points of bounding box corners using a PnP algorithm. Finally, a CNN per object is trained to refine the pose. By using multiple separated CNNs, BB8 is not end-to-end and is time-consuming for the inference. Similar to [25], in the recent technical report [32], the authors extend YOLO object detection network [26] to predict 2D projections of the corners of the 3D bounding boxes around objects. Given the projected 2D coordinates and the 3D ground control points of bounding box corners, a PnP algorithm is further used to estimate the 6D object pose.

RPN-based detection and segmentation. One of key components in the recent successful object detection method

Faster R-CNN [27] and instance segmentation method Mask R-CNN [9] is the Region Proposal Network — RPN. The core idea of RPN is to dense sampling the whole input image by many overlap bounding boxes at different shapes and sizes. The network is trained to produce multiple object proposals (also known as Region of Interest — RoI). This design of RPN allows to smoothly search over different scales of feature maps. Faster R-CNN [27] further refines and classifies RoIs with additional fully connected layers, while Mask R-CNN [9] further improves over Fast R-CNN by segmenting instances inside RoIs with additional convolutional layers.

In this paper, we go beyond Mask RCNN. In particular, depart from the backbone of Mask R-CNN, we propose a novel head branch which takes RoIs from RPN as inputs to regress the 6D object poses and is parallel with the existing branches. This results a novel end-to-end architecture which is not only detecting, segmenting but also directly recovering the 6D poses of object instances from a single RGB image.

III. METHOD

Our goal is to simultaneously detect, segment, and estimate the 6D poses of object instances in the input image. Mask R-CNN performs well for the first two tasks, except the 6D pose estimation. In order to achieve a complete system, we propose a novel branch which takes RoIs from RPN as inputs and outputs the 6D poses of the instances inside the RoIs. Although the concept is simple, the additional 6D pose is distinct from the other branches. It requires an effective way to represent the 6D pose and a careful design of the loss function. In this paper, we represent a pose by a 4-dimensional vector, in which the first three elements represent the Lie algebra associated with the rotation matrix of the pose; the last element represents the z component of the translation vector of the pose. Given the predicted z component and the predicted bounding box from the box regression branch, we use projective property to recover the full translation vector. The architecture of Deep-6DPose is shown in Figure 1.

A. Deep-6DPose

Let us first briefly recap Mask R-CNN [9]. Mask R-CNN consists of two main components. The first component is a RPN [27] which produces candidate RoIs. The second component extracts features from each candidate RoI using RoIAlign layer [9] and performs the classification, the bounding box regression, and the segmentation. We refer readers to [9] for details of Mask-RCNN.

Deep-6DPose also consists of two main components. The first component is also a RPN. In the second component, in parallel to the existing branches of Mask R-CNN, Deep-6DPose also outputs a 6D pose for the objects inside RoIs.

a) Pose representation: An important task when designing the pose branch is the representation space of the output poses. We learn the translation in the Euclidean space. In stead of predicting full translation vector, our network is trained to regress the z component only. The reason is that when projecting a 3D object model into a 2D image, two

translation vectors with the same z and the different x and y components may produce two objects which have very similar appearance and scale in 2D image (at different positions in the image – in the extreme case of parallel projection, there is no difference at all). This causes difficulty for the network to predict the x and y components by using only appearance information as input. However, the object size and the scale of its textures in a 2D image provide strong cues about the z -coordinate. This projective property allows the network to learn the z component of the translation using the 2D object appearance only. Given the z component, it is used together with predicted bounding box, which is outputted by the bounding box regression branch, to fully recover the translation. The detail of this recovering process is presented in the following sections.

Representing the rotation part of the pose is more complicated than the translation part. Euler angles are intuitive due to the explicit meaning of parameters. However, the Euler angles wrap around at 2π radians, i.e., having multiple values representing the same angle. This causes difficulty in learning a uni-modal scalar regression task. Furthermore, the Euler angles-based representation suffers from the well-studied problem of gimbal lock [3]. Another alternative, the use of 3×3 orthonormal matrix is over-parametrised, and creates the problem of enforcing the orthogonality constraint when training the network through back-propagation. A final common representation is the unit length 4-dimensional quaternion. One of the downsides of quaternion representation is its norm should be unit. This constraint may harm the optimization [15].

In this work, we use the Lie algebra $so(3)$ associated with the Lie group $SO(3)$ (which is space of 3D rotation matrices) as our rotation representation. The Lie algebra $so(3)$ is known as the tangent space at the identity element of the Lie group $SO(3)$. We choose the Lie algebra $so(3)$ to represent the rotation because an arbitrary element of $so(3)$ admits a skew-symmetric matrix representation parameterized by a vector in \mathbb{R}^3 which is continuous and smooth. This means that the network needs to regress only three scalar numbers for a rotation, without any constraints. To our best knowledge, this paper is the first one which uses Lie algebra for representing rotations in training a deep network for 6D object pose estimation task.

During training, we map the groundtruths of rotation matrices to their associated elements in $so(3)$ by the closed form Rodrigues logarithm mapping [2]. The mapped values are used as regression targets when learning to predict the rotation.

In summary, the pose branch is trained to regress a 4-dimensional vector, in which the first three elements represent rotation part and the last element represents the z component of the translation part of the pose.

b) Multi-task loss function: In order to train the network, we define a multi-task loss to jointly train the bounding box class, the bounding box position, the segmentation, and the pose of the object inside the box. Formally, the loss function

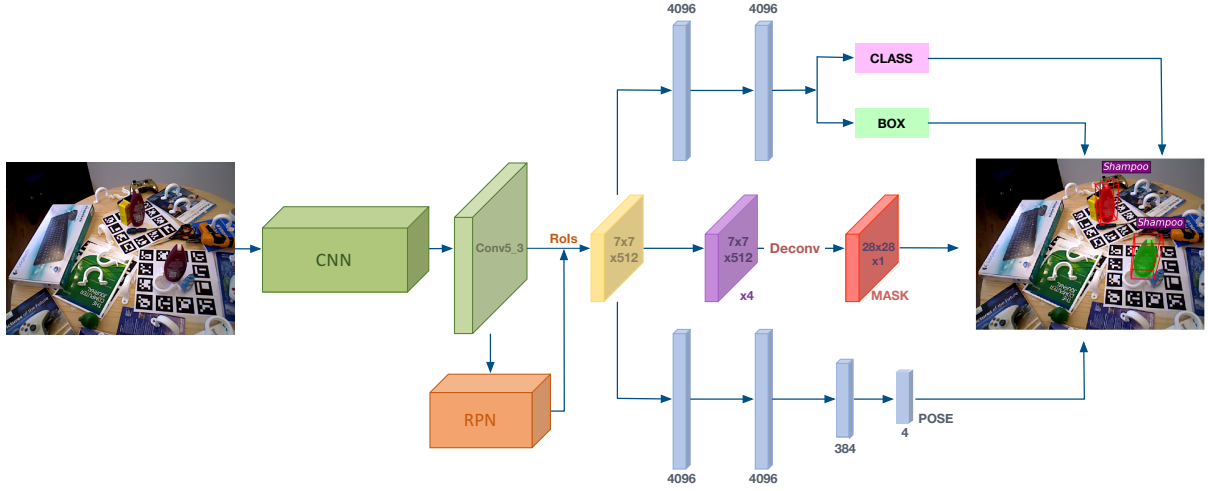


Fig. 1. An overview of Deep-6DPose framework. From left to right: The input to Deep-6DPose is a RGB image. A deep CNN backbone (i.e., VGG) is used to extract features over the whole image. The RPN is attached on the last convolutional layer of VGG (i.e., *conv5_3*) and outputs RoIs. For each RoI, the corresponding features from the feature map *conv5_3* are extracted and pooled into a fixed size 7×7 . The pooled features are used as inputs for 4 head branches. For the box regression and classification heads, we follow Mask-RCNN [9]. The segmentation head is *adapted* from [9], i.e., four 3×3 consecutive convolutional layers (denoted as ‘ $\times 4$ ’) are used. The ReLu is used after each convolutional layer. A deconvolutional layer is used to upsample the feature map to 28×28 which is the segmentation mask. The proposed pose head consists of four fully connected layers. The ReLu is used after each of the first three fully connected layers. The last fully connected layer outputs four numbers which represent for the pose. As shown on the right image, the network outputs the detected instances (with classes, i.e., Shampoo), the predicted segmentation masks (different object instances are shown with different colors) and the predicted 6D poses for detected instances (shown with 3D boxes).

is defined as follows

$$L = \alpha_1 L_{cls} + \alpha_2 L_{box} + \alpha_3 L_{mask} + \alpha_4 L_{pose} \quad (1)$$

The classification loss L_{cls} , the bounding box regression loss L_{box} , and the segmentation loss L_{mask} are defined similar as [9], which are *softmax* loss, *smooth L1* loss, and *binary cross entropy* loss, respectively. The $\alpha_1, \alpha_2, \alpha_3, \alpha_4$ coefficients are scale factors to control the important of each loss during training.

The pose branch outputs 4 numbers for each RoI, which represents the Lie algebra for the rotation and z component of the translation. It is worth noting that in our design, the output of pose branch is class-agnostic, but the class-specific counterpart (i.e., with a $4C$ -dimensional output vector in which C is the number of classes) is also applicable. The pose regression loss L_{pose} is defined as follows

$$L_{pose} = \|r - \hat{r}\|_p + \beta \|t_z - \hat{t}_z\|_p \quad (2)$$

where r and \hat{r} are two 3-dimensional vectors representing the **regressed rotation and the groundtruth rotation**, respectively; t_z and \hat{t}_z are two scalars representing the regressed z and the groundtruth z of the translation; p is a distance norm; β is a scale factor to control the rotation and translation regression errors.

c) *Network architecture*: Figure 1 shows the schematic overview of Deep-6DPose. We differentiate two parts of the network, i.e., the backbone and the head branches. The backbone is used to extract features over the whole image and is shared between head branches. There are four head branches corresponding to the four different tasks, i.e., the bounding box regression, the bounding box classification, the

segmentation, and the 6D pose estimation for the object inside the box. For the backbone, we follow Faster R-CNN [27] which uses VGG [30] together with a RPN attached on the last convolutional layer of VGG (i.e., *conv5_3*). For each output RoI of RPN, a fixed-size 7×7 feature map is pooled from the *conv5_3* feature map using the RoIAlign layer [9]. This pooled feature map is used as input for head branches. For the network heads of the bounding box regression and classification, we closely follow the Mask R-CNN [9]. For the segmentation head, we adapt from Mask R-CNN. In our design, four 3×3 consecutive convolutional layers (denoted as ‘ $\times 4$ ’ in Figure 1) are used after the pooled feature map. The ReLu is used after each convolutional layer. A deconvolutional layer is used to upsample the feature map to 28×28 which is the segmentation mask. **It is worth noting that for segmentation head, we use the class-agnostic design, i.e., this branch outputs a single mask, regardless of class.** We empirically found that this design reduces the model complexity and the inference time, while it is nearly effective as the class-specific design. This observation is consistent with the observation in Mask R-CNN [9].

In order to adapt the shared features to the specific pose estimation task, the pose head branch consists of a sequence of 4 fully connected layers in which the number of outputs are $4096 \rightarrow 4096 \rightarrow 384 \rightarrow 4$. **The ReLU is used after each fully layer, except for the last layer.** This is because the regressing targets (i.e., the groundtruths) contain both negative and positive values. We note that our pose head has a simple structure. More complex design may have potential improvements.

B. Training and inference

a) *Training*: We implement Deep-6DPose using Caffe deep learning library [12]. The input to our network is a RGB image with the size 480×640 . The RPN outputs RoIs at different sizes and shapes. We use 5 scales and 3 aspect ratios, resulting 15 anchors in the RPN. The 5 scales are 16×16 , 32×32 , 64×64 , 128×128 and 256×256 ; the 3 aspect ratios are $2 : 1$, $1 : 1$, $1 : 2$. This design allows the network to detect small objects.

The $\alpha_1, \alpha_2, \alpha_3$, and α_4 in (1) are empirically set to 1, 1, 2, 2, respectively. The values of β in (2) is empirically set to 1.5. An important choice for the pose loss (2) is the regression norm p . Typically, deep learning models use $p = 1$ or $p = 2$. With the datasets used in this work, we found that $p = 1$ give better results and hence is used in our experiments.

We train the network in an end-to-end manner using stochastic gradient descent with 0.9 momentum and 0.0005 weight decay. The network is trained on a Titan X GPU for 350k iterations. Each mini batch has 1 image. The learning rate is set to 0.001 for the first 150k iterations and then decreased by 10 for the remaining iterations. The top 2000 RoIs from RPN (with a ratio of 1:3 of positive to negative) are subsequently used for computing the multi-task loss. A RoI is considered positive if it has an intersection over union (IoU) with a groundtruth box of at least 0.5 and negative otherwise. The losses L_{mask} and L_{pose} are defined for only positive RoIs.

b) *Inference*: At the test phase, we run a forward pass on the input image. The top 1,000 RoIs produced by the RPN are selected and fed into the box regression and classification branches, followed by non-maximum suppression [7]. Based on the outputs of the classification branch, we select the outputted boxes from the regression branch that have classification scores higher than a certain threshold (i.e., 0.9) as the detection results. The segmentation branch and the pose branch are then applied on the detected boxes, which output segmentation masks and the 6D poses for the objects inside the boxes.

c) *From the 4-dimensional regressed pose to the full 6D pose*: Given the predicted Lie algebra, i.e., the first three elements of the predicted 4-dimensional vector from pose branch, we use the exponential Rodrigues mapping [2] to map it to the corresponding rotation matrix. In order to recover the full translation, we rely on the predicted z component (t_z – the last element of the 4-dimensional predicted vector) and the predicted bounding box coordinates to compute two missing components t_x and t_y . We assume that the bounding box center (in 2D image) is the projected point of the 3D object center (the origin of the object coordinate system). Under this assumption, using the 3D-2D projection formulation, we compute t_x and t_y as follows

$$t_x = \frac{(u_0 - c_x)t_z}{f_x} \quad (3)$$

$$t_y = \frac{(v_0 - c_y)t_z}{f_y} \quad (4)$$

where u_0, v_0 are the bounding box center in 2D image, and the matrix $[f_x, 0, c_x; 0, f_y, c_y; 0, 0, 1]$ is the known intrinsic camera calibration matrix.

IV. EXPERIMENTS

We evaluate Deep-6DPose on two widely used datasets, i.e., the single object pose dataset LINEMOD provided by Hinterstoisser et al. [10] and the multiple object instance pose dataset provided by Tejani et al. [31]. We also compare Deep-6DPose to the state-of-the-art methods for 6D object pose estimation from RGB images [5, 25, 13].

Metric: Different 6D pose measures have been proposed in the past. In order to evaluate the recovered poses, we use the *standard* metrics used in [5, 25]. To measure pose error in 2D, we project the 3D object model into the image using the groundtruth pose and the estimated pose. The estimated pose is accepted if the IoU between two project boxes is higher than 0.5. This metric is called as *2D-pose metric*. To measure the pose error in 3D, the *5cm5°* and *ADD* metrics is used. In *5cm5°* metric, an estimated pose is accepted if it is within 5cm translational error and 5° angular error of the ground truth pose. In *ADD* metric, an estimated pose is accepted if the average distance between transformed model point clouds by the groundtruth pose and the estimated pose is smaller than 10% of the object's diameter. We also provide the *F1* score of the detection and segmentation results. A detection / segmentation is accepted if its IoU with the groundtruth box / segmentation mask is higher than a threshold. We report results with the widely used thresholds, i.e., 0.5 and 0.9 [27, 9].

A. Single object pose estimation

In [10], the authors publish LINEMOD, a RGBD dataset, which has become a *de facto* standard benchmark for 6D pose estimation. The dataset contains poorly textured objects in a cluttered scene. We only use the RGB images to evaluate our method. The dataset contains 15 object sequences. For fair comparison to [5, 25, 13], we evaluate our method on the 13 object sequences for which the 3D models are available. The images in each object sequence contain multiple objects, however, only one object is annotated with the groundtruth class label, bounding box, and 6D pose. The camera intrinsic matrix is also provided with the dataset. Using the given groundtruth 6D poses, the object models, and the camera matrix, we are able to compute the groundtruth segmentation mask for the annotated objects. We follow the evaluation protocol in [5, 25] which uses RGB images from the object sequences for training and testing. For each object sequence, we randomly select 30% of the images for training and validation. The remaining images serve as the test set. A complication when using this dataset for training arises because not all objects in each image are annotated, i.e., only one object is annotated per sequence, even though multiple objects are present. This is problematic for training a detection/segmentation network such as [27, 9] because the training may be confused, e.g. slow or fail to converge, if an object is annotated as foreground in some images and as background other images. Hence, we preprocess the

	Ape	Bvise	Cam	Can	Cat	Driller	Duck	Box	Glue	Holep	Iron	Lamp	Phone	Average
Detection Segmentation	IoU 0.5													
	99.8	100	99.7	100	99.5	100	99.8	99.5	99.2	99.0	100	99.8	100	99.7
Detection Segmentation	IoU 0.9													
	99.5	99.8	99.7	100	99.1	100	99.4	99.5	99.0	98.6	99.2	99.4	99.7	99.4
Detection Segmentation	85.4	91.7	93.3	93.6	89.3	87.5	86.3	94.2	81.1	93.2	92.5	91.3	90.8	90.0
	80.6	57.0	91.4	62.5	52.1	74.6	81.2	91.9	73.3	84.6	90.3	85.0	84.6	77.6

TABLE I
F1 SCORE FOR 2D DETECTION AND SEGMENTATION OF DEEP-6DPOSE ON LINEMOD DATASET [10] FOR SINGLE OBJECT.

	Ape	Bvise	Cam	Can	Cat	Driller	Duck	Box	Glue	Holep	Iron	Lamp	Phone	Average
Deep-6DPose Brachmann[5] SSD-6D[13]	2D-pose metric													
	99.8	100	99.7	100	99.2	100	99.8	99.0	97.1	98.0	99.7	99.8	99.1	99.3
	98.2	97.9	96.9	97.9	98.0	98.6	97.4	98.4	96.6	95.2	99.2	97.1	96.0	97.5
Deep-6DPose Brachmann[5] BB8[25]	5cm5° metric													
	-	-	-	-	-	-	-	-	-	-	-	-	-	99.4
	57.8	72.9	75.6	70.1	70.3	72.9	67.1	68.4	64.6	70.4	60.7	70.9	69.7	68.5
Deep-6DPose Brachmann[5] BB8[25]	ADD metric													
	34.4	40.6	30.5	48.4	34.6	54.5	22.0	57.1	23.6	47.3	58.7	49.3	26.8	40.6
	80.2	81.5	60.0	76.8	79.9	69.6	53.2	81.3	54.0	73.1	61.1	67.5	58.6	69.0
Deep-6DPose Brachmann[5] BB8[25] SSD-6D[13]	38.8	71.2	52.5	86.1	66.2	82.3	32.5	79.4	63.7	56.4	65.1	89.4	65.0	65.2
	33.2	64.8	38.4	62.9	42.7	61.9	30.2	49.9	31.2	52.8	80.0	67.0	38.1	50.2
	40.4	91.8	55.7	64.1	62.6	74.4	44.3	57.8	41.2	67.2	84.7	76.5	54.0	62.7
	-	-	-	-	-	-	-	-	-	-	-	-	-	76.3

TABLE II
POSE ESTIMATION ACCURACY ON THE LINEMOD DATASET [10] FOR SINGLE OBJECT.



Fig. 2. Qualitative results for single object pose estimation on the LINEMOD dataset [10]. From left to right: (i) original images, (ii) the predicted 2D bounding boxes, classes, and segmentations, (iii) 6D poses in which the green boxes are the groundtruth poses and the red boxes are the predicted poses. Best view in color.

training images as follows. For each object sequence, we use the RefineNet [19], a state-of-the-art semantic segmentation algorithm, to train a semantic segmentation model. The trained

model is applied on all training images in other sequences. The predicted masks in other sequences are then filtered out, so that the appearance of the objects without annotated information

does not hinder the training.

Results: Table I presents the 2D detection and segmentation results of Deep-6DPose. At an IoU 0.5, the results show that both detection and segmentation achieve nearly perfect scores for all object categories. This reconfirms the effective design of Faster R-CNN [27] and Mask R-CNN [9] for object detection and instance segmentation. When increasing the IoU to 0.9, both detection and segmentation accuracy significantly decrease. The more decreasing is observed for the segmentation, i.e., the dropping around 10% and 22% for detection and segmentation, respectively.

We put our interest on the pose estimation results, which is the main focus of this work. Table II presents the comparative pose estimation accuracy between Deep-6DPose and the state-of-the-art works of Brachmann et al. [5], BB8 [25], SSD-6D [13] which also use RGB images as inputs to predict the poses. Under *2D-pose* metric, Deep-6DPose is comparable to SSD-6D, while outperforms over [5] around 2%. Under *5cm5°* metric, Deep-6DPose is slightly lower than BB8, while it significantly outperforms [5], i.e., around 28%. Under ADD metric, Deep-6DPose outperforms BB8 2.5%. The results of Deep-6DPose are also more stable than BB8 [25], e.g., under *5cm5°* metric, the standard deviations in the accuracy of Deep-6DPose and BB8 [25] are 5.0 and 10.6, respectively. The Table II also shows that both Deep-6DPose and BB8 [25] are worse than SSD-6D. However, it is worth noting that SSD-6D [13] does not use images from the object sequences for training. The authors [13] perform a discrete sampling over *whole* rotation space and use the known 3D object models to generate synthetic images used for training. By this way, the training data of SSD-6D is able to cover more rotation space than [5], BB8 [25], and Deep-6DPose. Furthermore, SSD-6D also further uses an ICP-based refinement to improve the accuracy. Different from SSD-6D, Deep-6DPose directly outputs the pose without any post-processing. Figure 2 shows some qualitative results of Deep-6DPose for single object pose estimation on the LINEMOD dataset.

B. Multiple object instance pose estimation

In [31], Tejani et al. publish a dataset consisting of six object sequences in which the images in each sequence contain multiple instances of the same object with different levels of occlusion. Each object instance is provided with the groundtruth class label, bounding box, and 6D pose. Using the given groundtruth 6D poses, the object models, and the known camera matrix, we are able to compute the groundtruth segmentation masks for object instances. We use the RGB images provided by the dataset for training and testing. We randomly split 30% images in each sequence for training and validation. The remaining images serve as the test set.

Results: The 2D detection and segmentation results are presented in Table III. At an IoU 0.5, Deep-6DPose achieves nearly perfect scores. When increasing the IoU to 0.9, the average accuracy decreases around 10% and 14% for detection and segmentation, respectively. We found that the Shampoo category has the most drop. It is caused by its flat shape, e.g.,

at some certain poses, the projected 2D images only contain a small side edge of the object, resulting the drop of scores at high IoU.

The accuracy of the recovered poses is reported in Table IV. Under *2D-pose* metric, both Deep-6DPose and SSD-6D [13] achieve mostly perfect scores. Under *5cm5°* and ADD metrics, on the average, Deep-6DPose achieves 64.5% and 62.0% accuracy, respectively. We note that no previous works reports the standard *5cm5°* and ADD metrics on this dataset using only RGB images. Figure 3 shows some qualitative results for the predicted bounding boxes, classes, segmentations, and 6D poses for multiple object instances.

We also found that Deep-6DPose is not very robust to nearly rotationally symmetric objects. That is because if an object is rotational symmetry in *z* axis, any rotation of the 3D object in the Yaw angle will produce the same object appearance in the 2D image. This makes confusion for the network to predict the rotation using only appearance information. As shown in Table IV, the Coffee sequence, which is nearly rotational symmetry in both shape and texture, has very low *5cm5°* score. Figure 4 shows a failure case for this object sequence.

C. Timing

When testing on the LINEMODE dataset [10], Brachman et al. [5] reports a running time around 0.45s per image. Deep-6DPose is several times faster than their method, i.e., its end-to-end architecture allows the inference at around 0.1s per image on a Titan X GPU. SSD-6D [13] and BB8 [25] report the running time around 0.1s and 0.3s per image, respectively. Deep-6DPose is comparable to SSD-6D in the inference speed, while it is around 3 times faster than BB8. It is worth noting that due to using post-refinement, the inference time of SSD-6D and BB8 may be increased when the input image contains multiple object instances. We note that although Deep-6DPose is fast, its parameters are still not optimized for the speed. As shown in the recent study [11], better trade-off between speed and accuracy may be achieved by carefully selecting parameters, e.g., varying the number of proposals after RPN, image sizes, which is beyond scope of the current work.

V. CONCLUSION

In this paper, we propose Deep-6DPose, a deep learning approach for jointly detecting, segmenting, and most importantly recovering 6D poses of object instances from an single RGB image. Deep-6DPose is end-to-end trainable and can directly output estimated poses without any post-refinements. The novelty design is at a new pose head branch, which uses the Lie algebra to represent the rotation space. Deep-6DPose compares favorably with the state-of-the-art RGB-based 6D object pose estimation methods. Furthermore, Deep-6DPose also allows a fast inference which is around 10 fps. An interesting future work is to improve the network for handling with rotationally symmetric objects.

	Camera	Coffee	Joystick	Juice	Milk	Shampoo	Average
Detection Segmentation	99.8	100	99.8	IoU 0.5 99.2	99.7	99.5	99.6
	99.8	99.7	99.6	99.0	99.3	99.5	99.4
Detection Segmentation	88.3	97.2	97.7	IoU 0.9 89.4	83.5	82.4	89.7
	81.7	95.0	95.5	86.9	77.8	74.7	85.2

TABLE III

F1 SCORE FOR 2D DETECTION AND SEGMENTATION OF DEEP-6DPOSE ON THE DATASET OF TEJANI ET AL. [31] FOR MULTIPLE OBJECT INSTANCES.

	Camera	Coffee	Joystick	Juice	Milk	Shampoo	Average
Deep-6DPose SSD-6D[13]	2D pose metric						
	99.2	100	99.6	98.4	99.5	99.1	99.3
Deep-6DPose	-	-	-	-	-	-	98.8
	5cm5° metric						
Deep-6DPose	76.5	18.7	60.2	85.6	73.5	72.4	64.5
	ADD metric						
Deep-6DPose	80.4	35.4	27.5	81.2	71.6	75.8	62.0

TABLE IV

POSE ESTIMATION ACCURACY ON THE DATASET OF TEJANI ET AL. [31] FOR MULTIPLE OBJECT INSTANCES.



Fig. 3. Qualitative results for pose estimation on the multiple object instance dataset of Tejani et al. [31]. From left to right: (i) the original images, (ii) the predicted 2D bounding boxes, classes, and segmentations (different instances are shown with different colors), (iii) 6D poses in which the green boxes are the groundtruth poses and the red boxes are the predicted poses. Best view in color.



Fig. 4. One fail case on the Coffee sequence in the dataset of Tejani et al. [31]. Although the network can correctly predict the bounding box, the estimated 6D is incorrect due to the rotational symmetry of the object. We can see that the incorrect rotations are mainly in the Yaw axis.

REFERENCES

- [1] Motilal Agrawal. A Lie algebraic approach for consistent pose registration for general euclidean motion. In *IROS*, 2006.
- [2] C. Altafini. The de casteljau algorithm on $SE(3)$. In *Nonlinear control in the Year 2000*, 2000.
- [3] S. L. Altmann. *Rotations, quaternions, and double groups*. Courier Corporation, 2005.
- [4] Eric Brachmann, Alexander Krull, Frank Michel, Stefan Gumhold, Jamie Shotton, and Carsten Rother. Learning 6D object pose estimation using 3D object coordinates.

- In *ECCV*, 2014.
- [5] Eric Brachmann, Frank Michel, Alexander Krull, Michael Ying Yang, Stefan Gumhold, and Carsten Rother. Uncertainty-driven 6D pose estimation of objects and scenes from a single RGB image. In *CVPR*, 2016.
 - [6] Thanh-Toan Do, Anh Nguyen, Ian D. Reid, Darwin G. Caldwell, and Nikos G. Tsagarakis. AffordanceNet: An end-to-end deep learning approach for object affordance detection. In *ICRA*, 2018.
 - [7] Ross B. Girshick. Fast R-CNN. In *ICCV*, 2015.
 - [8] Iryna Gordon and David G. Lowe. What and where: 3D object recognition with accurate pose. In *Toward Category-Level Object Recognition*, 2006.
 - [9] Kaiming He, Georgia Gkioxari, Piotr Dollár, and Ross B. Girshick. Mask R-CNN. In *ICCV*, 2017.
 - [10] Stefan Hinterstoisser, Vincent Lepetit, Slobodan Ilic, Stefan Holzer, Gary R. Bradski, Kurt Konolige, and Nassir Navab. Model based training, detection and pose estimation of texture-less 3D objects in heavily cluttered scenes. In *ACCV*, 2012.
 - [11] Jonathan Huang, Vivek Rathod, Chen Sun, Menglong Zhu, Anoop Korattikara, Alireza Fathi, Ian Fischer, Zbigniew Wojna, Yang Song, Sergio Guadarrama, and Kevin Murphy. Speed/accuracy trade-offs for modern convolutional object detectors. In *CVPR*, 2017.
 - [12] Yangqing Jia, Evan Shelhamer, Jeff Donahue, Sergey Karayev, Jonathan Long, Ross B. Girshick, Sergio Guadarrama, and Trevor Darrell. Caffe: Convolutional architecture for fast feature embedding. In *ACM MM*, 2014.
 - [13] Wadim Kehl, Fabian Manhardt, Federico Tombari, Slobodan Ilic, and Nassir Navab. SSD-6D: making rgb-based 3D detection and 6D pose estimation great again. In *ICCV*, 2017.
 - [14] Alex Kendall and Roberto Cipolla. Geometric loss functions for camera pose regression with deep learning. In *CVPR*, 2017.
 - [15] Alex Kendall, Matthew Grimes, and Roberto Cipolla. PoseNet: A convolutional network for real-time 6-dof camera relocation. In *ICCV*, 2015.
 - [16] Alex Krizhevsky, Ilya Sutskever, and Geoffrey E Hinton. Imagenet classification with deep convolutional neural networks. In *NIPS*, 2012.
 - [17] Alexander Krull, Eric Brachmann, Frank Michel, Michael Ying Yang, Stefan Gumhold, and Carsten Rother. Learning analysis-by-synthesis for 6D pose estimation in RGB-D images. In *ICCV*, 2015.
 - [18] Alexander Krull, Eric Brachmann, Sebastian Nowozin, Frank Michel, Jamie Shotton, and Carsten Rother. PoseAgent: Budget-constrained 6D object pose estimation via reinforcement learning. In *CVPR*, 2017.
 - [19] G. Lin, A. Milan, C. Shen, and I. Reid. RefineNet: Multi-path refinement networks for high-resolution semantic segmentation. In *CVPR*, 2017.
 - [20] Wei Liu, Dragomir Anguelov, Dumitru Erhan, Christian Szegedy, Scott E. Reed, Cheng-Yang Fu, and Alexander C. Berg. SSD: single shot multibox detector. In *ECCV*, 2016.
 - [21] Jonathan Long, Evan Shelhamer, and Trevor Darrell. Fully convolutional networks for semantic segmentation. In *CVPR*, 2015.
 - [22] David G. Lowe. Distinctive image features from scale-invariant keypoints. *IJCV*, pages 91–110, 2004.
 - [23] Manuel Martinez, Alvaro Collet, and Siddhartha S. Srinivasa. MOPED: A scalable and low latency object recognition and pose estimation system. In *ICRA*, 2010.
 - [24] Frank Michel, Alexander Kirillov, Eric Brachmann, Alexander Krull, Stefan Gumhold, Bogdan Savchynskyy, and Carsten Rother. Global hypothesis generation for 6D object pose estimation. In *CVPR*, 2017.
 - [25] Mahdi Rad and Vincent Lepetit. BB8: A scalable, accurate, robust to partial occlusion method for predicting the 3D poses of challenging objects without using depth. In *ICCV*, 2017.
 - [26] Joseph Redmon and Ali Farhadi. YOLO9000: better, faster, stronger. In *CVPR*, 2017.
 - [27] Shaoqing Ren, Kaiming He, Ross B. Girshick, and Jian Sun. Faster R-CNN: towards real-time object detection with region proposal networks. In *NIPS*, 2015.
 - [28] Reyes Rios-Cabrera and Tinne Tuytelaars. Discriminatively trained templates for 3D object detection: A real time scalable approach. In *ICCV*, 2013.
 - [29] Germán Ros, Julio Guerrero, Angel Domingo Sappa, Daniel Ponsa, and Antonio Manuel López Peña. VS-LAM pose initialization via Lie groups and Lie algebras optimization. In *ICRA*, 2013.
 - [30] Karen Simonyan and Andrew Zisserman. Very Deep Convolutional Networks for Large-Scale Image Recognition. *CoRR*, 2014.
 - [31] Alykhan Tejani, Danhang Tang, Rigas Kouskouridas, and Tae-Kyun Kim. Latent-class hough forests for 3D object detection and pose estimation. In *ECCV*, 2014.
 - [32] Bugra Tekin, Sudipta N. Sinha, and Pascal Fua. Real-time seamless single shot 6D object pose prediction. *arXiv*, Nov, 2017.
 - [33] Yu Xiang, Tanner Schmidt, Venkatraman Narayanan, and Dieter Fox. PoseCNN: A convolutional neural network for 6D object pose estimation in cluttered scenes. *arXiv*, Nov, 2017.